*Technology and Science for the Ships of the Future*
*V. Crupi and V. Bucci (Eds.)*

*doi:10.3233/PMST250003*

# Optimal Geometry of ABH-Based Honeycomb Panels for Vibro-Acoustic Control on Board Cruise Ships

Giada KYAW OO D'AMORE [a,1], Francesco MAURO [a], Giovanni ROGNONI [a], Jacopo BARDIANI [b] and Marco BIOT [a]
[a] *University of Trieste, Department of Engineering and Architecture, Trieste, Italy*
[b] *Polytechnic of Milan, Department of Mechanical Engineering, Milano, Italy*
ORCiD ID: Giada Kyaw Oo D'Amore https://orcid.org/0000-0001-5587-4280
Francesco Mauro https://orcid.org/0000-0003-3471-9411
Giovanni Rognoni https://orcid.org/0000-0002-3864-9724
Jacopo Bardiani https://orcid.org/0000-0003-4572-8073
Marco Biot https://orcid.org/0009-0009-4674-5618

**Abstract.** The control of both structure-borne noise and airborne noise is of paramount importance on board cruise ships. The international regulations limit the noise levels in the ship's surroundings and internal spaces. Moreover, the classification societies release different comfort classes based on the noise levels ensured in the cabins, and of course, the owners would like to reach the highest class. For such reasons, researching innovative solutions to improve vibro-acoustic control onboard ships is of primary interest to the maritime industry. Honeycomb panels are usually used as soundproofing ceilings on board ships; therefore, this paper aims to increase their performance by embedding Acoustic Black Holes (ABH) in their geometry. The ABHs are a technology capable of capturing and reducing the vibrations of the structure on which they are applied. Different research reported in the literature demonstrates their efficiency and proposes some applications, for example, in the automotive sector. As the ABH effect depends not only on the ABH size but also on its shape, the most efficient ABH profile inside a honeycomb panel has been determined. The obtained results highlight the validity of the adopted procedure and give guidelines for the design of ABH-based panels to improve soundproofing on board cruise ships.

**Keywords.** Vibro-acoustic control, Acoustic Black Holes, Ship Comfort, Honeycomb Panels, Numerical Optimization

## 1. Introduction

Noise on board ships is an issue for both passengers and crew. International regulations limit the noise levels in the different spaces of the ship to safeguard people's health [1]. Moreover, shipowners' requests are increasingly stringent to obtain the highest comfort classes, defined by the classification societies [2], so that the ship can be considered a luxury one, leading to high profitability for the shipowners.

[1] Corresponding Author: Giada Kyaw Oo D'Amore, giada.kyawood'amore@dia.units.it, Via Alfonso Valerio 6, 34127 Trieste, Italy

Accordingly, the analysis of the noise sources on board ships [3–5] and alternative solutions to noise control and attenuation [6] become of paramount importance.

Public areas and cabins are usually insulated using insulating panels, ceilings and technical floors (*e.g.,* floating floors). In such a way, the control of both airborne noise and structural-borne noise is reached.

Specifically, ceilings made of mineral wool coupled to aluminium honeycomb panels are typically used to ensure proper aero-acoustic insulation. However, mineral wool is considered a dangerous material for both the environment and operators' health [7] and has been classified in UE as "carcinogen Category 2 and assigned the hazard phrase H351: "Suspected of causing cancer" [8]. Thus, the reduction of its usage is a target in shipbuilding. Moreover, the noise levels required by the shipowners are increasingly restrictive and strategies to improve the acoustic insulation are needed.

In the recent decade, there has been an increasing number of studies on the use of Acoustic Black Holes (ABHs) as a novel device able to achieve damping of flexural vibrations in engineering structures [9], thus reducing the radiated noise [10]. Different configurations and geometries are proposed [10] and their Technology Readiness Level (TRL) is considered equal to 3 [11]. Noticeably, reports on the application of ABHs in the marine field are missing.

This paper investigates the feasibility of embedding ABH in a honeycomb panel aiming at reducing its radiated noise. The efficiency of the addressed solution is evaluated through a Finite Element Method (FEM) simulation, using the vibrations of the panel as Key Performance Index (KPI). From a systematic variation of the main geometrical parameters of the ABH, it has been possible to identify the most suitable ABH's geometry to maximise the vibration dissipation.

## 2. ABH-based honeycomb panel

A traditional ceiling used on board ships is composed of aluminium honeycomb panels composed of two aluminum sheets of 1 mm thick and a honeycomb core of 8 mm. The honeycomb core usually has hexagonal cells with a hydraulic diameter of 6 mm.

In the presented study, an ABH is embedded inside the honeycomb panel to reduce the acoustic radiation and thus improve its insulating properties. Such technology can be adopted as alternative solution to traditional ceiling, especially where noise sources have high levels. For example, the insulation of public areas like theater to ensure high comfort levels in the above cabins is a challenge on board passenger ships.

In the following sections, the ABH principle is briefly described, and the modelling strategy for the ABH-based honeycomb panel is addressed.

### *2.1. ABH principle*

ABHs were first studied by Mironov [12], who described the phenomenon whereby flexural waves channelled into a tapered beam or plate are dissipated with no reflection at the edge. The thickness of the ABH cannot go to zero at the tip for construction reasons. This causes a reflection of the flexural waves that are not completely dissipated by the ABH itself. Thus, viscoelastic materials are applied in the ABH region to dissipate the vibrational energy.

The ABH profile is created by reducing the thickness of the structure following a power law profile described by the following equation:

$$h(x) = \frac{H-h}{L^N} x^N + h \tag{1}$$

where $H$, $h$, and $L$ are the ABH dimensions (Figure 1) and $N$ is greater than or equal to 2. This profile generates an exponential decrease in the velocity of the incident wave with the propagation distance. The kinetic energy entrapped in the region of low velocity can be dissipated using absorbing materials [13].

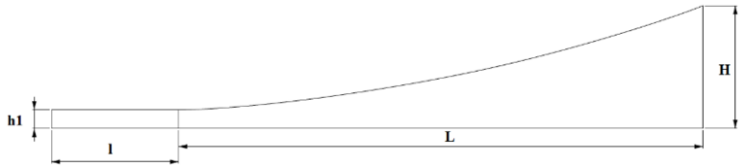


**Figure 1.** ABH shape outlines.

The length of the ABH depends on the cut-on frequency above which the desired effect occurs. The cut-on frequency can be expressed as follows [10]:

$$f_{cut-on} = \frac{h}{2\pi L^2} \sqrt{\frac{E(40-24\nu)}{12\rho(1-\nu^2)}} \tag{2}$$

where $E$, $\rho$ and $\nu$ are the Young Modulus, the density and the Poisson ratio of the solid material, respectively.

### *2.2. FEM modelling*

To study the effect of the embedded ABH, just a portion of the honeycomb panel is modelled using symmetry boundary conditions. In Figure 2, the meshed geometry is reported. The mesh size is chosen in order to have at least 8 linear elements per smallest wavelength. A constrained viscoelastic layer is applied in the ABH region to increase the wave dissipation. The ABH is designed with a cut-on frequency of approximately 50 Hz (Eq. 2). Since the panel is composed of materials with different mechanical characteristics (*i.e.*, aluminum sheets and honeycomb core), equivalent values of $E$, $\rho$ and $\nu$ are used to estimate the cut-on frequency. Such values are calculated as the average of those of the considered materials and re-proportioned to their thickness. In Tables 1, 2 and 3, the mechanical characteristics of the materials are reported (η and G are respectively the loss factor and the shear modulus). The honeycomb core is modelled as a transversely isotropic material.

**Table 1.** Mechanical characteristics of aluminum.

| E [GPa] | η [-] | ν [-] | ρ [kg·m-3] |
|---|---|---|---|
| 70 | 0.01 | 0.3 | 2700 |

**Table 2.** Mechanical characteristics of aluminum honeycomb.

| E plane [MPa] | ν plane [-] | G plane [MPa] | E norm [MPa] | ν norm [-] | ρ [kg·m-3] | η [-] |
|---|---|---|---|---|---|---|
| 3 | 0.95 | 30 | 150 | 0.3 | 75 | 0.01 |

**Table 3.** Mechanical characteristics of viscoelastic material.

| E [MPa] | η [-] | ν [-] | ρ [kg·m-3] |
|---|---|---|---|
| 60 | 0.9 | 0.4 | 1200 |

**Figure 2.** ABH model: blue-honeycomb, pink-viscoelastic layer, grey-aluminium, red-control points, green-point load.

A direct frequency response analysis is performed in the frequency range 0-1000 Hz. A point load is applied in the node highlighted in green in Figure 2. The model is clamped along the shorter edge with homogeneous thickness. The displacements as a function of frequency are evaluated in the red points in Figure 2 and the medium values are used for comparisons. As a matter of fact, the lower the displacements on the panel's region with uniform thickness, the higher is the energy dissipated by the ABH region, and the lower is the radiated noise by the panel's surfaces.

## 3. Design Strategy

A Response Surface Methodology (RSM) [14] is implemented to optimize the ABH geometry in order to minimize the vibration of the panel. The RSM involves three fundamental steps: design a series of experiments to evaluate the analyzed response, creation of a mathematical model that fits the response, analysis of the optimum conditions.

The displacements evaluated in the uniform thickness region of the honeycomb panel are used for comparison. In particular, the maximum peak value with the replated frequency and the area under the curve of the displacement as a function of frequency are considered as KPI.

### *3.1. Design Space Creation*

Design of Experiment (DoE) techniques allow for creating a database of displacements as a function of predetermined parameters needed to construct the metamodel. The predictor parameters, with their constraints, constitute the design space.

The power coefficient $N$ of the ABH's profile (Eq. 1), the minimum thickness of the ABH $h$, and the length $l$ of the prolongation at the ABH's tip (Figure 1) are selected as predictor parameters in the presented study. The Box–Behnken designs [15] is adopted for the determination of simulation scenarios. In Table 4, the upper and lower limits for

the predictor parameters are reported. Such limits are imposed by the following considerations: overall dimensions of the panel for $l$, minimum and maximum $h_1$ dictated by the panel and aluminum sheet thicknesses, and manufacturing difficulties for too high $m$ values.

**Table 4.** Minimum and maximum values for the predictor parameters.

| N [-] | h [mm] | l [mm] |
|---|---|---|
| 2-22 | 2-10 | 0-415 |

In Table 5 the performed simulations are reported. It should be noticed that configurations 8-14 are not modelled due to errors related to the discretization of the geometry caused by a honeycomb core too thin at the tip of the ABH. The honeycomb is modelled with solid elements and with very thin layer the quality of the mesh is too poor to perform the calculations.

Other simulations are then addressed to better cover the design space, having at least two simulations with the same $N$ and $h_1$, while $l$ changes. The configuration 42 represents the uniform honeycomb panel.

**Table 5.** Minimum and maximum values for the predictor parameters.

| Configuration | h [mm] | l [mm] | N [-] | Configuration | h [mm] | l [mm] | N [-] |
|---|---|---|---|---|---|---|---|
| 1 | 2 | 0 | 2 | 22 | 4.5 | 0 | 14 |
| 2 | 2 | 207.5 | 2 | 23 | 4.5 | 207.5 | 14 |
| 3 | 2 | 415 | 2 | 24 | 4.5 | 415 | 14 |
| 4 | 2 | 0 | 6 | 25 | 4.5 | 0 | 18 |
| 5 | 2 | 415 | 6 | 26 | 4.5 | 207.5 | 18 |
| 6 | 2 | 0 | 10 | 27 | 4.5 | 415 | 18 |
| 7 | 2 | 207.5 | 10 | 28 | 4.5 | 0 | 22 |
| 8 | 2 | 0 | 14 | 29 | 4.5 | 415 | 22 |
| 9 | 2 | 207.5 | 14 | 30 | 6 | 0 | 2 |
| 10 | 2 | 415 | 14 | 31 | 6 | 207.5 | 2 |
| 11 | 2 | 0 | 18 | 32 | 6 | 415 | 2 |
| 12 | 2 | 207.5 | 18 | 33 | 6 | 0 | 6 |
| 13 | 2 | 415 | 18 | 34 | 6 | 207.5 | 6 |
| 14 | 2 | 207.5 | 22 | 35 | 6 | 415 | 6 |
| 15 | 4.5 | 0 | 2 | 36 | 6 | 0 | 10 |
| 16 | 4.5 | 415 | 2 | 37 | 6 | 207.5 | 10 |
| 17 | 4.5 | 0 | 6 | 38 | 6 | 207.5 | 14 |
| 18 | 4.5 | 207.5 | 6 | 39 | 6 | 0 | 18 |
| 19 | 4.5 | 0 | 10 | 40 | 6 | 415 | 18 |
| 20 | 4.5 | 207.5 | 10 | 41 | 6 | 207.5 | 22 |
| 21 | 4.5 | 415 | 10 | 42 | 10 | 0 | 2 |

In Figures 3 the displacement curves as a function of frequency are reported. For the sake of conciseness, only the curves relative to the configurations 1, 2, 4, 15 and 42 (*i.e.*, the standard honeycomb panel) are reported as an example. It is already possible to notice from the Figures 3 how the displacement curves are strongly influenced by the presence of the ABH and by the variation of its parameters.

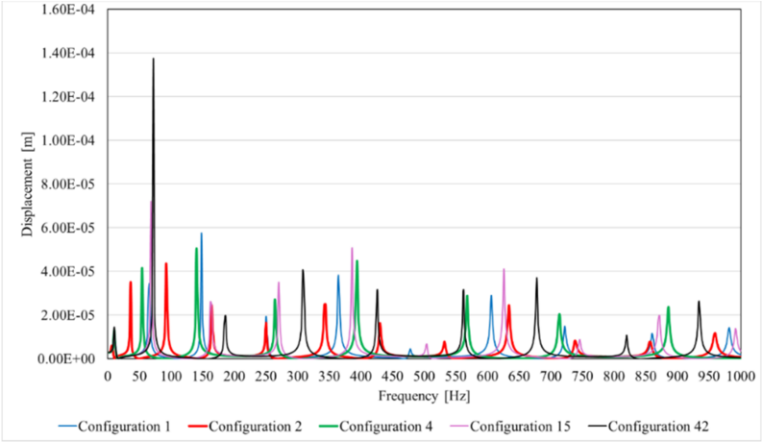


**Figure 3.** Displacements vs frequency in narrow band.

### *3.2. Surrogate models and optimal geometries*

After the database generation, a surrogate model is necessary for the prediction of both the maximum peak value with the related frequency and the area under the displacement curves. The latter values are calculated considering the curves in a 1/3 octave band, while the peaks are evaluated considering the curves in a narrow band. Surrogate models have been generated through Multiple Linear Regression (MLR) techniques [16].

MLR is a commonly used statistical technique that aims to model the relationship between a dependent variable $Y$ and several independent variables $X_i$. In essence, MLR attempts to fit a linear equation to observed data to predict or understand the dependencies of the dependent variable on the predictors. This method is a natural extension of simple linear regression, where there is only one predictor. By incorporating more predictors, MLR enables researchers to explore complex relationships between variables, making it a powerful tool in various fields such as economics, social sciences, medicine, and engineering. In MLR, the dependent variable $Y$ is modeled as a linear combination of multiple independent variables. The general form of the model is:

$$Y = \beta_0 + \sum_{i=1}^{N_p} \beta_i X_i + \varepsilon \tag{3}$$

where $Y$ is the dependent variable, $X_i$ are the $N_p$ predictors (the independent variables), $\beta_i$ are the regression coefficients, $\beta_0$ is the model intercept, and $\varepsilon$ is the regression error.

The goal in multiple linear regression is to estimate the coefficients $\beta_0, \beta_1, \ldots, \beta_{Np}$ so that the residual sum of squares (RSS) is minimized.

After obtaining the coefficients, it is essential to evaluate the model's performance. Common metrics include the determination coefficient $R^2$ and the adjusted determination coefficient $R^2_{adj}$.

The MLR technique can also be applied by considering different combinations between independent variables, up to considering polynomial functions of them. Here, a complete 4th-order polynomial model has been applied to the three independent variables of the process ($N$, $l$ and $h$), adopting a procedure which automatically excludes the non-significant predictors, thus finding the minimum number of significant predictors for each regression.

The above-described process has been applied to the maximum peak value, the peak frequency and the area under the displacement curve. The results do not provide a good model for the maximum peak value and the peak frequency. In fact, the values for the determination coefficient $R^2$ are significantly low. For the maximum peak value, a model with 8 coefficients has been determined, resulting in an $R^2$ of 0.4193 and an $R^2_{adj}$ of 0.2567. For the peak frequency, the model has 21 terms, with an $R^2$ of 0.6126 and an $R^2_{adj}$ of 0.0010. Therefore, the two regressions are not significant, highlighting that the maximum peak value and its associated frequency are not correlated with the geometrical parameters of the ABH.

The case is different for the area of the displacement curve. Here, MLR gave a better correlation between the dependent and independent variables, with an $R^2$ of 0.9171 and an $R^2_{adj}$ of 0.8603 (model with 14 parameters). However, the regression model is quite significant only for values of $N$ up to 12. High $N$ values highlight negative values of the displacement areas in the extremes of the calculation domain, which is unfeasible. This may be due to the problems observed in the modelling of ABH already described above, leading to an incomplete filling of the originally planned design space.

However, even though the obtained model is valid for a reduced number of $N$ values, it could still give some useful indications for the design of ABH. Figure 4 shows, as an example, the response surface of the maximum peak value for the values of $N$ equal to 2, 4 and 6. The resulting surface derived from the MLR analysis highlights a strong

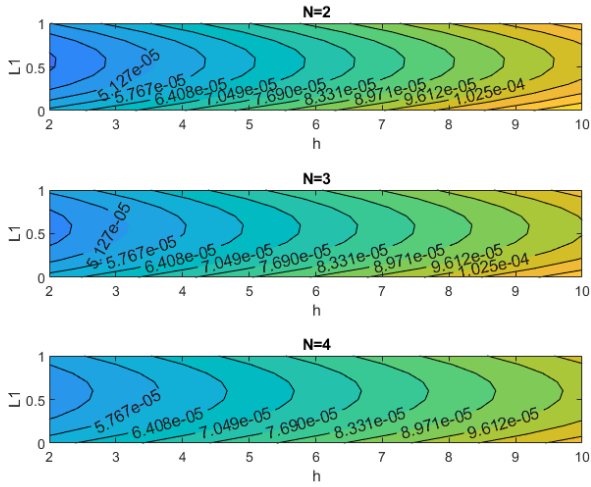


**Figure 4.** Response surfaces of the maximum peak value at different values of N. l is expressed as ratio of L and named L1.

dependence of the maximum peak value on the independent variables. For each *N*, the area corresponding to the minimum value is clearly visible, allowing to find the most favorable combinations of *l* and *h* to minimize the peak.

Figure 5 shows the response surface for the displacement area at the *N* values of 2, 4 and 6. Also, in this case, the surface highlights a strong dependence of the displacement area on the three independent variables. The surface allows for identifying the most favorable combinations of *l* and *h* to minimize the displacement area. It can be immediately seen that the geometry combinations that are optimal for the maximum peak value are quite the same as those for the displacement area.

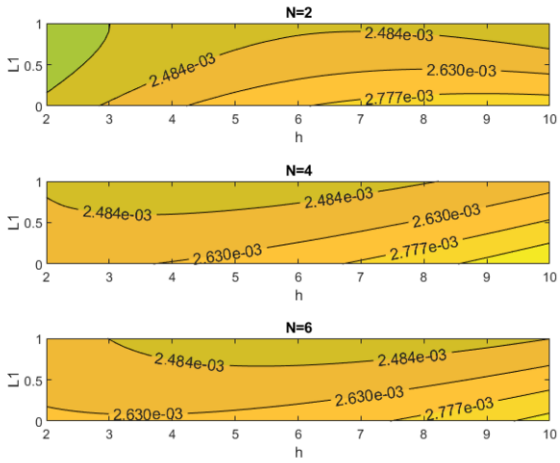


**Figure 5**. Response surface of the displacement area at different values of N. l is expressed as ratio of L and named L1.

As the MLRs are polynomial formulations as a function of the independent variables, determining the optimum combinations of *N*, *l* and *h* is straightforward, and does not require the implementation of complex optimization algorithms. Both maximum peak value and displacement area are quantities to minimize, thus the problem is reduced to the search for the global optimum. The only constraints applied to the model are the limitations on the variables reported in Table 4, with the additional limitation on *N* discussed above to avoid unfeasible solutions.

As a result, the optimal configurations for both the peak value and the displacement area are N=2, h=2 mm and l=207.5 mm.

Figure 6 shows the comparison of the displacement curve of the optimized ABH with the reference one, highlighting the reduction of the amplitudes along the whole frequency range.

In any case, the present study is an exploratory research in the field, thus requiring further analysis to better refine the design space for the generation of the surrogate models needed for optimization. Furthermore, it is not yet clear what design constraints are needed for the practical realization of an ABH, resulting in constraints to put in the optimum geometry research process. Notwithstanding the above, the present work is surely a step further in the understanding of ABH applicability to the maritime sector.

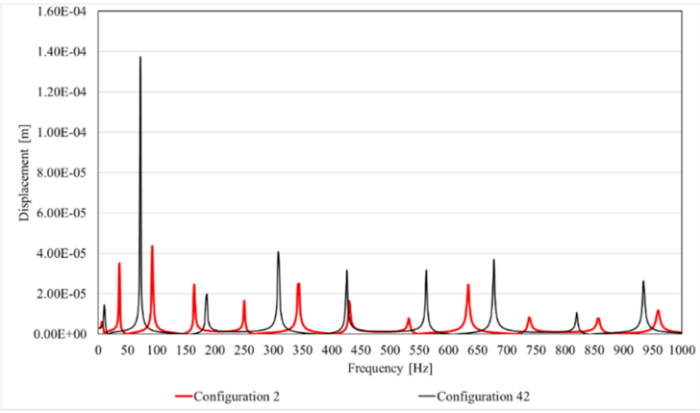


**Figure 6**. Optimal ABH geometry (up) and displacement curves comparison (down)

## 4. Conclusion

The present work presented an exploratory study for the determination of the optimum geometry parameters of a honeycomb ABH for marine applications. Starting from a conventional geometry for an ABH, three geometrical parameters have been found as fundamental for defining a parametric geometry.

The application of DoE techniques, in the specific a Box-Behnken methodology, made it possible to generate a design space of ABHs by changing the geometrical parameters systematically. The geometries have then been analyzed with dedicated FEM analyses, extracting values of engineering interest like the maximum peak and the displacement area. This allows for generating a database of data, starting point for the execution of MLR as a function of the main geometrical parameters of the ABH. MLRs highlight a good quality of fit only for the case of the displacement area. The models have limitations due to geometrical modeling problems, leading to an incomplete coverage of the initial design space.

In any case, also on a reduced design space it was possible to determine the optimal geometry for the ABH, searching for the geometrical parameters minimizing the displacement area. This geometry is able to minimize also the maximum peak value.

Even though the study is preliminary, it represents a good starting point for the development of future studies covering a broader design space, with better coverage of the geometrical parameters, avoiding unfeasible geometries. The obtained results, even though preliminary and explorative, represent a step towards a better understanding of the applicability of ABH in the maritime industry.

In future real case studies should be considered, both numerically and experimentally, to further investigate the ABH properties in noise control. They could be a valuable solution to improve the insulations of public areas to ensure high comfort on board ships.

## References

[1] IMO, Code on Noise Level On Board Ships - Res. A.468(XII), 2012.

[2] RINA, Rules for the classification of ships., 2018. https://www.rina.org/it/rules (accessed January 11, 2018).

[3] D. Borelli, T. Gaggero, E. Rizzuto, and C. Schenone, Analysis of noise on board a ship during navigation and manoeuvres, *Ocean Engineering*. 105 (2015) 256–269. doi:10.1016/j.oceaneng.2015.06.040.

[4] T. Ozawa, M. Hirakata, T. Tsukada, S. Suda, S. Abe, and T. Takahashi, Optimization of Hull Structure and Noise Control Measures for Noise in Accommodation Space, *J.JASNAOE*. 30 (2019) 177–185. doi:10.2534/jjasnaoe.30.177.

[5] D. Borelli, T. Gaggero, E. Rizzuto, and C. Schenone, Onboard ship noise: Acoustic comfort in cabins, *Applied Acoustics*. 177 (2021) 107912. doi:10.1016/j.apacoust.2021.107912.

[6] G. Kyaw Oo D'Amore, S. Caverni, M. Biot, G. Rognoni, and L. D'Alessandro, A Metamaterial Solution for Soundproofing on Board Ship, *Applied Sciences*. 12 (2022) 6372. doi:10.3390/app12136372.

[7] P. Harrison, P. Holmes, R. Bevan, K. Kamps, L. Levy, and H. Greim, Regulatory risk assessment approaches for synthetic mineral fibres, *Regulatory Toxicology and Pharmacology*. 73 (2015) 425–441. doi:10.1016/j.yrtph.2015.07.029.

[8] M. Kupczewska-Dobecka, K. Konieczko, and S. Czerczak, Occupational risk resulting from exposure to mineral wool when installing insulation in buildings, *International Journal of Occupational Medicine and Environmental Health*. 33 (2020) 757–769. doi:10.13075/IJOMEH.1896.01637.

[9] B.M.P. Chong, L.B. Tan, K.M. Lim, and H.P. Lee, A Review on Acoustic Black-Holes (ABH) and the Experimental and Numerical Study of ABH-Featured 3D Printed Beams, *Int. J. Appl. Mechanics*. 09 (2017) 1750078. doi:10.1142/S1758825117500788.

[10] A. Pelat, F. Gautier, S.C. Conlon, and F. Semperlotti, The acoustic black hole: A review of theory and applications, *Journal of Sound and Vibration*. 476 (2020) 115316. doi:10.1016/j.jsv.2020.115316.

[11] T.A. Smith, and J. Rigby, Underwater radiated noise from marine vessels: A review of noise reduction methods and technology, *Ocean Engineering*. 266 (2022) 112863. doi:10.1016/j.oceaneng.2022.112863.

[12] Mironov, Propagation of a flexural wave in a plate whose thickness decreases smoothly to zero in a finite interval, *Sov. Phys. Acoust.* 34 (1988) 318–319.

[13] V.V. Krylov, Propagation of plate bending waves in the vicinity of one- and two-dimensional acoustic 'black holes,' (2007). doi:10.13140/RG.2.1.4425.6484.

[14] M. Farooq Anjum, I. Tasadduq, and K. Al-Sultan, Response surface methodology: A neural network approach, *European Journal of Operational Research*. 101 (1997) 65–73. doi:10.1016/S0377-2217(96)00232-9.

[15] Box, G., Hunter, W., and Hunter, J., Statistics for experiments: Design, Innovation, and Discovery, II nd, Wiley Interscience, New York, 2005.

[16] G.A.F. Seber, and A.J. Lee, Linear Regression Analysis, 2nd ed., Wiley, 2023.